CORROSION BEHAVIOR OF STEEL BAR EMBEDDED IN ALKALI-ACTIVATED SLAG CONCRETE SUBJECTED TO CARBONATION AND CHLORIDE ATTACK

COMPORTAMIENTO FRENTE A LA CORROSIÓN DEL ACERO EMBEBIDO EN CONCRETO DE ESCORIA ACTIVADO ALCALINAMENTE SOMETIDO A CARBONATACION Y ATAQUE A IÓN CLORURO

WILLIAN APERADOR CHAPARRO

Ph.D. Profesor, Ingeniería Mecatrónica, Universidad Militar Nueva Granada, g.ing.materiales@gmail.com

ENRIQUE VERA LÓPEZ

Ph.D. Profesor, Escuela de Metalurgia, Universidad Pedagógica y Tecnológica de Colombia

RUBY MEJÍA DE GUTIÉRREZ

Ph.D. Profesora, Escuela de Ingeniería de Materiales (GMC), Universidad del Valle

Received for review October 21 th, 2009, accepted October 10th, 2010, final version October, 15 th, 2010

ABSTRACT: This paper presents an experimental study on the corrosion resistance of a steel bar embedded in an alkali-activated slag (AAS) concrete in which it was exposed to an accelerated carbonation test (3% CO_2, 65% relative humidity (RH), and 25 ºC) and then tested under complete immersion in 3.5 wt. % NaCl solution. Ordinary Portland cement (OPC) was also tested for comparative purposes and was exposed to identical experimental conditions. The monitoring of open-circuit potential, the linear polarization resistance technique, and the electrochemical impedance spectroscopy (EIS), were used to evaluate the corrosion behavior of the steel bar. Corrosion resistance of carbonated AAS and OPC concretes was tested at different times. We carried out an exposure test of a solution containing Cl ions with all series for 0, 3, 6, 9, and 12 months. Electrochemical measurements show that AAS concrete presents depassivation of the steel embedded in concrete where it is exposed to accelerated carbonation; after this period of time, corrosion resistance decreased due to the presence of chlorides at the steel/AAS interface.

KEYWORDS: alkali-activated cement, chloride ion, electrochemical measurements

RESUMEN: Este trabajo presenta el estudio experimental de la resistencia a la corrosión de la barra de acero embebida en el concreto obtenido de la escoria siderúrgica activada alcalinamente (AAS) el concreto se expone a ensayos de carbonatación acelerada (3% de CO2, 65% de humedad relativa (HR), y 25 ºC) y una inmersión en solución de cloruro de sodio al 3,5%. El concreto Portland ordinario tipo I se utilizó con propósitos comparativos y fue expuesto a las mismas condiciones experimentales. La evaluación de la corrosión de las barras de acero se hizo mediante medidas de potencial de circuito abierto (OCP), resistencia a la polarización lineal (LPR) y espectroscopia de impedancias electroquímica (EIS). La resistencia a la corrosión de los concretos AAS y OPC se evaluaron a diferentes tiempos. Se llevó a cabo una prueba de exposición de una solución que contiene iones Cl con todas las muestras a los 0, 3, 6, 9 y 12 meses. Los ensayos electroquímicos muestran que el concreto AAS presenta despasivacion acero debido a la exposición a la carbonatación acelerada, después de este periodo de tiempo, posteriormente la resistencia a la corrosión decrece debido a la presencia del ion cloruro en la interfase acero / AAS.

PALABRAS CLAVE: concreto de activación alcalina, ion cloruro, medidas electroquímicas.

1. INTRODUCTION

The nature and integrity of the layer of solid hydration products formed in close to embedded steel may have an important role in controlling the passivation and depassivation of the metal [1]. However, these reinforcements suffer severe corrosion problems when the reinforced concrete structure is exposed to chloride-contaminated environments and/or when the concrete cover is carbonated. Chlorides favor localized pitting corrosion of the steel, and the effect of carbonation by the penetration of CO_2 in relation to the corrosion of the reinforcement is given by reducing the pH of the water pore. The drop in pH at certain levels can cause

the loss of first passive, the initiation of corrosion, and, over time, severe corrosion of the reinforcement [2–5].

Corrosion of steel bar damages the reinforced concrete structures in two ways: First, it reduces the cross-sectional area of the steel bar. Secondly, it produces corrosion products with a larger volume than the steel itself. The volume increase induces the tensile stress in concrete, which results in cracking and eventual structural failure [6,7].

Granulated blast-furnace slag (GBFS) has been used for many years as a supplementary cementitious material (SCM) in ordinary Portland cement (OPC) concrete, either as a mineral admixture or as a component of blended cement [6]. Doubts have been raised about the use of GBFS in pre-stressed and post-tensioned concrete. The GBFS contains sulphides that can catalyze the development of hydrogen atoms when pre-stressed steel embedded in concrete corrodes; thus leading to hydrogen embrittlement. Nevertheless, tests and practical experience for over 50 years have shown that such a concern is not justified and that GBFS cement can be used freely [7].

The very high temperatures (1400–1500 ºC) required in manufacturing OPC, which make it responsible for 40% of all energy consumed, account for the extremely high cost of this process. The environmental impact attributed to OPC manufacturing is largely due to the energy-intensive processes involved. Indeed, the cement industry is regarded as responsible for 6–7% of all world-wide greenhouse gases emitted [8].

In an attempt to overcome these problems, the construction sector is interested in developing new cement binding materials as an alternative to OPC [9]. In this respect, the most promising approach emerging is based on raw materials suitable for alkaline activation, from which originate new binding materials generically known as *alkaline cements* [10]. Granulated blast-furnace slag undergoes rapid hydration when mixed with an appropriate trigger such as a sodium silicate solution, and, if mixed with aggregates, it can produce a dense and airtight concrete that presents high mechanical strength at early ages [11–12].

Granulated blast-furnace slags are the result of the combination of acid iron clay and the sulphurous ashes of coke (also with acid properties) with lime and dolomite limestone by melting at high temperatures (~1600 ºC), and cooling the magmatic fluid from 1400 °C to room temperature [13–14].

Considering that rebar corrosion is the main cause of reinforced concrete structure (RCS) failure [15–17], the capacity of alkali-activated slag (AAS) concretes to passivate steel rebars is an important issue for guaranteeing the durability of RCS constructed with these materials. The passivating capacity and the permanence of the passive state, once reached, depend on the nature and the dosage of the binder, as well as on environmental conditions.

The aim of this paper is to study the corrosion properties of steel rebars embedded in artificially carbonated AAS (3% CO_2) and concrete exposed to a chloride solution. For comparative purposes, steel rebars were embedded in OPC under identical experimental conditions. The specimens were studied by using corrosion potential, linear polarization resistance, and electrochemical impedance spectroscopy methods.

2. EXPERIMENTAL SET-UP

Granulated blast-furnace slag from the company *Acerías Paz del Río*, located in Boyacá, Colombia, was used with a chemical composition (% by weight) of 33.7 SiO_2, 12.8 Al_2O_3, 3.09 Fe_2O_3, 45.4 CaO, 0.5 TiO_2, 0.64 SO_3, 1.79 MgO, and 2.08 loss on ignition; a specific surface area of 398 $m^2\ kg^{-1}$; and a specific gravity of 2860 kg m^{-3}. The basicity ($CaO + MgO / SiO_2 + Al_2O_3$) and quality ($CaO + MgO + Al_2O_3 / SiO_2 + TiO_2$) indexes were 1.01 and 1.73, respectively. According to the ASTM C 989-99 standard, this material was grade 80 slag [18]. The waterglass used as the activating solution consisted of a mix of commercial sodium silicate (31.7% SiO_2, 12.3% Na_2O, and 56.0% water) with a 50% NaOH solution to obtain a SiO_2/Na_2O ratio of 2.4. The Na_2O concentration in the waterglass activating solution added to the concrete was 5% by weight of slag. The aggregate used was a siliceous gravel with 19-mm maximum grain size, a specific gravity of 2940 kg m^{-3}, and 1.3% absorption; and river sand with 19-mm maximum grain size, a specific gravity of 2470 kg m^{-3}, and 2.9% absorption. Ordinary Portland cement according to the ASTM C 150-02 standard was used for comparative purposes [19], with

a specific gravity and specific surface area of 2990 kg m^{-3} and 400 kg m^{-3}, respectively. Alkali-activated slag (AAS) and OPC concretes were prepared with a water/cement ratio of 0.4.

The AAS and OPC specimens were cured in a climatic cabinet for 28 days at 90% relative humidity (RH) for AAS specimens and at 100% RH for OPC specimens, to prevent leaching of the activating solutions and to assure that the hydration reaction and product formation processes were not affected.

Carbonation exposure was simulated by accelerated testing in a cabinet with 3% CO_2, 65% RH, and 25 ºC (AASA and OPCA specimens). After carbonation, the specimens were immersed in a chloride solution (3.5 wt. % NaCl) in order to test the effect of chloride contamination.

Structural 1018 steel bars of 6.35 mm diameter were used, according to the ASTM A 706-08 standard [20]. A cylindrical reinforced concrete specimen (76.2 mm diameter and 76.2 mm length) was used to perform the experimental tests.

Electrochemical measurements were carried out with a classic 3-electrode configuration, using the steel bars as a working electrode, a graphite bar as a counter electrode, and a copper/copper sulphate ($Cu/CuSO_4$) as reference electrode. An active 10-cm^2 surface area was marked on the working electrode with an epoxy resin; thus isolating the triple concrete/steel/atmosphere interface to avoid a possible localized corrosion attack due to differential aeration.

Steel bar corrosion over time was monitored by using three techniques: (a) Corrosion potential (E_{corr}) values in which the E_{corr} parameter may be used to define the probability of corrosion: for E_{corr} < -0.35 V vs. $Cu/CuSO_4$, high corrosion probability (~90%); for -0.35 V < E_{corr} < -0.20 V vs. $Cu/CuSO_4$, uncertainty of corrosion; and for E_{corr} > -0.20 V vs. $Cu/CuSO_4$, a 10% probability of corrosion [8,19]; (b) Linear polarization resistance (R_p) values ($R_p = \frac{\Delta E}{\Delta I}$). The steel corrosion rate can be calculated from the Stern-Geary equation [20]: $i_{corr} = \frac{B}{R_p}$, applying DE ± 20 mV at a scan rate of 0.16 mV s^{-1}, and by adopting a tentative value of 26 mV for the B constant. The corrosion level may be defined according to the Durar Network Specification [23]: for $i_{corr} < 0.1$ μA cm^{-2}, passivity; for 0.1 μA $cm^{-2} < i_{corr} < 0.5$ μA cm^{-2}, low corrosion; for 0.5 μA $cm^{-2} < i_{corr} < 1.0$ μA cm^{-2}, high corrosion; and for $i_{corr} > 1.0$ μA cm^{-2}, very high corrosion; and (iii) Electrochemical impedance spectroscopy (EIS), whose measurements were recorded at the E_{corr} in a frequency range from 1 ´ 10^5 Hz to 1 ´ 10^{-3} Hz with a logarithmic sweeping frequency of 3 points per decade. The EIS method involved the imposition of a 10 mV amplitude excitation voltage. A Gamry model PCI 4 workstation was utilised for DC and AC measurements. Electrochemical measurements were performed at 0, 15, 30, and 45 days (total carbonation of AASA specimens), and additionally at 60, 85, and 108 days for OPCA specimens. In order to be exposed to 3.5 wt. % NaCl, the measurements were performed at 0, 3, 6, 9, and 12 months for AAS and OPC specimens.

3. RESULTS AND DISCUSSION

Figure 1 shows the values of corrosion potential versus time for the steel bar embedded in AAS and OPC concrete. AAS concrete has a 10% probability of corrosion after 28 days of normal curing, once fully carbonated reaches a 90% with a potential of -0.51 V vs. $Cu/CuSO_4$. When this material is subsequently exposed to chloride, the corrosion potentials remain in the range between -0.51 and -0.56 V vs. $Cu/CuSO_4$, as is shown in Fig. 1. The high carbonation rate exhibited by AAS concrete may be attributed to the fact that the characteristic activation reactions after slag alkali activation are governed by dissolution and precipitation mechanisms, whose reaction kinetics are faster than the diffusion reactions that prevail in OPC hydration [24–25]. When dissolved species such as calcium, silicates, and aluminates reach the maximum concentration, they can precipitate, prompting the nucleation of the dissolved aluminates and silicates in an alkaline environment. These reactions generate depassivation steel corresponding to an active state based on the Pourbaix diagram. The active state is maintained for reinforcements during the 12-month exposure period. Portland cement concrete (OPC) shows a corrosion probability of 10% before exposure to chlorides, when it is exposed to accelerated carbonation, the corrosion potential lies in the range of -0.08 V to -0.4 V vs . $Cu/CuSO_4$, moving towards a 90% corrosion probability. Later, when exposed to chlorides for 12 months, this

potential decreases to -0.54 V vs. $Cu/CuSO_4$. In this case, OPC and AAS concretes have similar performance.

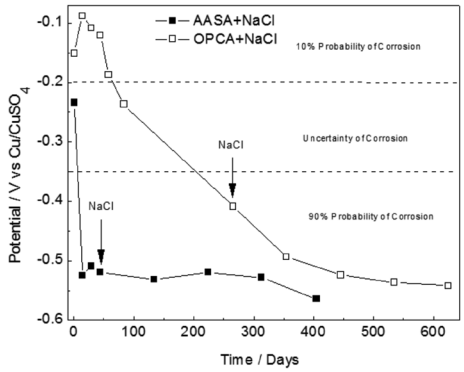

Figure 1. Corrosion potential (E_{corr}) versus time for steel rebars embedded in AAS and OPC concretes exposed to accelerated carbonation and exposed to chloride ions.

Figure 2 shows the polarization resistance of bars embedded in carbonated concrete and exposed to chloride. When the AAS concrete is totally carbonated (45 days of exposure to CO_2) the Rp value is reduced from Rp 23 kΩ cm^2 to 4.65 kΩ cm^2. This value is reduced to 0.71 kΩ cm^2 after exposure to a solution of 3.5 wt. % NaCl for 365 days. By contrast, OPC concrete in the first 60 days of carbonation process shows an increase of polarization resistance to values of 846 kΩ cm^2, then decreases. The full carbonation is reached at 265 days and thus the steel depassivation (Rp 50 kΩ cm^2). Finally, the presence of chlorides reduces Rp values to 13 kΩ cm^2 after 365 days of exposure. The corrosion currents at the end of the process of carbonation and chloride exposure, calculated based on the Stern Geary equation, are located at 2.36 mA cm^{-2} and 2 mA cm^{-2} for alkali-activated slag concrete (AAS) and OPC, respectively.

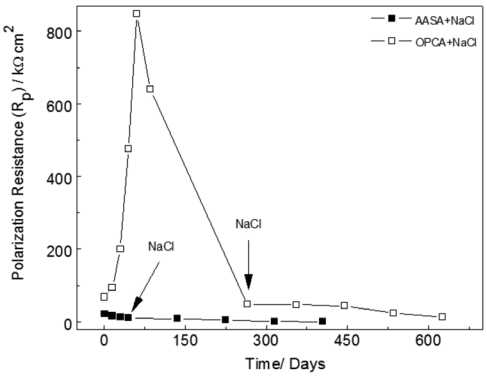

Figure 2. Polarization resistance (R_p) versus time for steel rebars embedded in AAS and OPC concretes with exposure to carbonation and chloride ions.

The results of AAS concrete show that the value of Rp decreases after 15 days of exposure because the high carbonation rate exhibited by AAS concrete may be attributed to the fact that the characteristic activation reactions after slag alkali activation are governed by a dissolution and precipitation mechanism whose kinetic reactions are faster than the diffusion reactions along water paths or open pores that prevail in OPC hydration [26–27]. These activation reactions lead to the formation of a gel of calcium silicate hydrate (CSH) characterized by a short-range order due to their low Ca/Si and the presence of Q3 type Si units [26]. Moreover, it has been reported that in AAS concrete, carbonation takes place directly on the C-S-H gel [29]. Alkali-activated slag concrete (AAS) concrete shrinks during the drying process, leading to the formation of microscopic cracks that facilitate the entry of CO_2 inside the concrete. Consequently, the interaction between CO_2 and this material leads to its decalcification and the loss of cohesion in the matrix [30]. It has been suggested that this unsuitability could be attenuated by grinding the slag much more finely and enhancing the efficiency of curing systems, proposing airtight systems with an average 90% RH. The AAS concrete performed better than the OPC concrete with respect to chloride penetrability.

The results for OPC concrete at accelerated carbonation may be due to the concrete hydration reactions, which under appropriate RH conditions can recur and generate the formation of a good protective layer on the steel surface. The presence of alkaline species such as KOH, NaOH, and $Ca(OH)_2$ seals the pores and gives rise to good corrosion resistance. Polarization resistance increased to 45 days of exposure, by which time CO_2 has already entered with a greater depth in the concrete but has not yet reached the concrete/steel interface. At 108 days of experimentation, the CO_2 front has reached the OPC concrete/steel interface and destroyed the passive layer, giving R_p values in the same order as that was measured at the start of the experiment. Then, when exposed to chlorides, the value of polarization resistance diminishes and the corrosion current increases as a result of acceleration of the corrosion process.

Figure 3 shows typical Nyquist plots for steel rebars embedded in concrete exposed to accelerated carbonation (AASA) and exposed to 3.5 wt. % NaCl. Measurements were performed at 0 days (AAS

specimen), 45 days (AASA), and at 180 and 360 days exposed to chloride. Table 1 includes fit data yielded by using the equivalent circuit from Fig. 4. In general, a capacitive behaviour was obtained, characterized by a poorly defined and depressed semicircle at high frequencies and a second semicircle associated with the steel corrosion process at low frequencies.

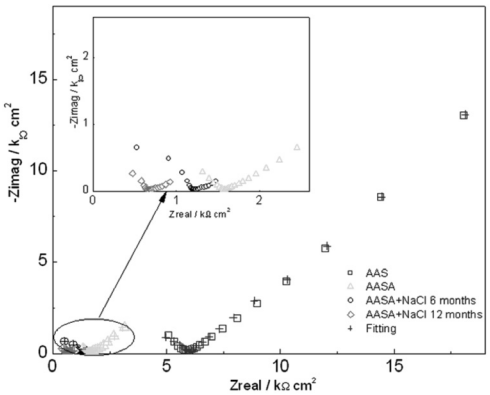

Figure 3. Nyquist plot experimentation for steel rebars embedded in AAS concrete exposed to accelerated carbonation (3% CO_2, 65% RH, 25 ºC) and 3.5% chloride.

The equivalent circuit in Fig. 4 contains two distributed constant phase elements (CPE_1 and CPE_2) to consider the two relaxation time constants (Figs. 3 and 5). The CPE_1–R_1 couple, which predominates at high frequencies, may be originated by the passive film and/or the dielectric properties of the concrete, while the CPE_2–R_2 couple, controlling at low frequencies, characterizes the corrosion process of the steel/concrete pore solution interface. R_Ω is the electrolyte resistance.

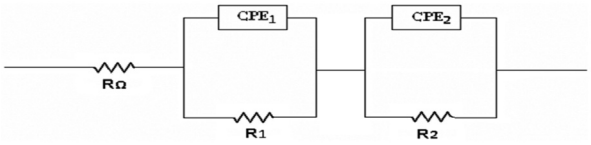

Figure 4. Electrical equivalent circuit used to fit impedance data of steel embedded in AAS and OPC concretes. R_Ω is the electrolyte/concrete interface resistance; CPE_1 and CPE_2 are constant phase elements defined at high and low frequency, respectively; R_1 is the pore solution resistance; and R_2 is the charge transfer resistance (corrosion).

Figure 5 shows typical Nyquist plots for steel rebars embedded in non-carbonated OPC concrete and in concrete exposed to accelerated carbonation (OPCA) for 108 days at 180 and 360 days exposed to chloride. Table 1 includes fit data yielded by using the equivalent circuit from Fig. 5. In general, as for AAS concrete, a capacitive behaviour was observed, characterized by a poorly defined semicircle at high frequencies and a second semicircle at low frequencies.

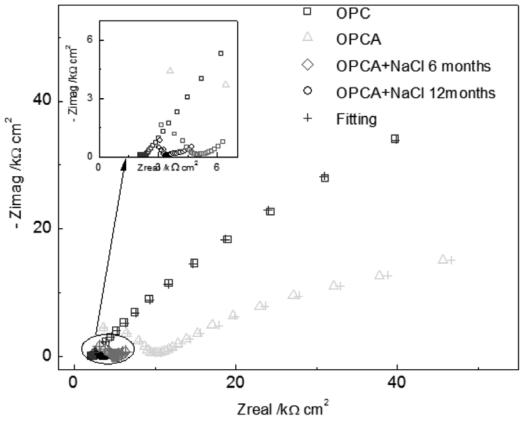

Figure 5. Nyquist plot experimentation for steel rebars embedded in OPC concrete exposed to accelerated carbonation (3% CO_2, 65% RH, 25 ºC) and 3.5% chloride.

Table 1 includes optimized fitting impedance parameter values for the AAS/steel and OPC/steel system. The high frequency process had a CPE_1 $\left(Y_{P_1}\right)$ in the range from 0.54 ´ 10^{-9} $Fcm^{-2}s^{-(1-\alpha_1)}$ to 15.5 ´ 10^{-6} $Fcm^{-2}s^{-(1-\alpha_1)}$. The optimized values for the various parameters are given in Table 1. For the OPC/steel system the high frequency process had a CPE_1 $\left(Y_{P_1}\right)$ in a range from 0.21 ´ 10^{-9} $Fcm^{-2}s^{-(1-\alpha_1)}$ to 20.13 ´ 10^{-6} $Fcm^{-2}s^{-(1-\alpha_1)}$.

The corrosion resistance (R2) for the AASA/steel system decreases with the time of exposure to accelerated carbonation and subsequent exposure to chlorides. By contrast, the OPC concrete specimens show a higher corrosion resistance at equal exposure conditions. (Table 1).

The fitting process gives a R_2 value from 505 kΩ cm² to 9 kΩ cm² for the AASA concrete, and 0.92 kΩ cm² for the AASA concrete exposed to chloride (Table 1). Accepting that the Stern-Geary equation can be applied, with an approximate B constant value of 26 mV, the resulting corrosion current density is high corrosion for AASA (i_{corr} = 2.8 μA cm^{-2}) and very high corrosion for AASA exposed to chloride (i_{corr} = 28 μA cm^{-2}), which

is not far from the i_{corr} results obtained by using the R_p measurements (Fig. 3b).

For the OPC/steel system, the EIS results show a depressed semicircle at high frequencies and a second semicircle also depressed at low frequencies, yielding an R_2 value from 177 kΩ cm^2 to 130 kΩ cm^2, for carbonated concrete, and 9.81 kΩ cm^2 for the OPCA exposed to chloride for 360 days; the estimated corrosion current density was very low for OPCA, at roughly 0.2 μA cm^{-2} and 2.6 μA cm^{-2}.

Table 1. Parameters used in the fitting of impedance data for steel rebars embedded in alkali-activated slag (AAS) and OPC concrete. The non-carbonated AAS and OPC specimens were exposed to accelerated carbonation (3% CO_2, 65% RH, 25 ºC) and 3.5% chloride.

Time Days	R_Ω Ω cm^2	Y_{P1} F cm^{-2} s$^{-(1-\alpha_1)}$	α_1	R_1 kΩ cm^2	Y_{P2} F cm^{-2} s$^{-(1-\alpha_2)}$	α_2	R_2 kΩ cm^2
Non-carbonated AAS Concrete							
0	200	0.54 ´ 10^{-9}	0.78	2.7	1.1 ´ 10^{-3}	0.59	505
AASA Concrete Exposed to Accelerated Carbonation							
45	64	1.28 ´ 10^{-9}	0.97	0.9	5.81 ´ 10^{-3}	0.55	9
AASA Concrete Exposed to Chloride							
90	8.3	56 ´ 10^{-6}	0.85	0.135	21 ´ 10^{-3}	0.85	1.82
180	5.2	48 ´ 10^{-6}	0.79	0.123	6.19 ´ 10^{-3}	0.92	1.47
270	4.7	37.6 ´ 10^{-6}	0.91	0.102	5.25 ´ 10^{-3}	0.76	1.26
360	4.7	15.5 ´ 10^{-6}	0.94	0.067	6.24 ´ 10^{-3}	0.88	0.92
Non-carbonated OPC Concrete							
0	63	0.21 ´ 10^{-9}	0.94	1.9	0.37 ´ 10^{-3}	0.63	177
OPCA Concrete Exposed to Accelerated Carbonation							
108	102	10 ´ 10^{-9}	0.90	8.1	0.12 ´ 10^{-3}	0.34	130
OPCA Concrete Exposed to Chloride							
90	23.2	26.58 ´ 10^{-6}	0.83	0.43	38.05 ´ 10^{-3}	0.86	44.72
180	31.4	26.3 ´ 10^{-6}	0.77	0.60	43.8 ´ 10^{-3}	0.79	26.31
270	30.8	18.92 ´ 10^{-6}	0.87	0.42	26.15 ´ 10^{-3}	0.92	14.67
360	25.3	20.13 ´ 10^{-6}	0.85	0.44	31.08 ´ 10^{-3}	0.78	9.81

4. CONCLUSIONS

Open-circuit potential evolution AAS concrete exposed to accelerated carbonation, showed a high corrosion, next to the one immersed in saline solution, indicating depassivation corrosion behaviour during the first 3 months. That would allow for us to predict the time for corrosion initiation on existing reinforced AAS concrete structures.

The steel embedded in OPC concrete without exposure to accelerated carbonation generates a non-uniform protective oxide coat. This coat disappears almost completely under aggressive conditions and at sites where it remains, porosity causes low metal protection. Under standard conditions, the AAS concrete presents a homogeneous oxide layer above the metal. However, upon exposure to chloride ions, a great part of this layer disappears obtaining small density. Nothing can be done in view of this corrosive attack, which validates the results obtained electrochemically.

ACKNOWLEDGEMENTS

W. Aperador expresses his gratitude to the Center of Excellence for Novel Materials (CENM) and COLCIENCIAS of Colombia, the Geoconcret Project, for the scholarship granted to him.

REFERENCES

[1] Puertas, F., Palacios, M., Vázquez, T., Carbonation process of alkali-activated slag mortars, J Mater Sci 41, pp. 3071-3082, 2006.

[2] Alien, J. S., Samuelson, R. and Newberger, A., Chaos in a model of forced quasi-geostrophic flow over topography: an application of Melinkov's method, J. Fluid Mech., 226, pp. 511-547, 1991.

[3] Wang, S.D., Scrivener, K.L., Hydration products of alkali activated slag cement, Cement Concrete Res 25, pp. 561-571, 1995.

[4] Palacios, M., Puertas, F., Effect of carbonation on alkali-activated slag paste. J Am Ceram Soc; 89: pp. 3211-3221, 2006.

[5] Shi, C., Strength, pore structure and permeability of alkali-activated slag mortars, Cement Concrete Res 26, pp. 1789-1799, 1996.

[6] Blanco, G., Bautista, A., Takenouti, H., EIS study of passivation of austenitic and duplex stainless steels reinforcements in simulated pore solutions. Cement and Concrete Composites 28, pp. 212–219, 2006.

[7] Song, H.W., Saraswanthy, V., Studies on the corrosion resistance of reinforced steel in concrete with ground granulated blast-furnace slag. An overview, J Hazard Mater 138, pp. 226-233, 2006.

[8] Bijen, J., Benefits of slag and fly ash, Constr Build Mater 10, pp. 309-314, 1996.

[9] Bastidas, D.M., Fernández-Jiménez, A., Palomo, González J.A., A study on the passive state stability of steel embedded in activated fly ash mortars, Corros Sci 50, pp. 1058-1065, 2008.

[10] Moreno, M., Morris, W., Alvarez, M.G., Duff, G.S., Corrosion of reinforcing steel in simulated concrete pore solutions. Effect of carbonation and chloride content, Corros Sci 46, pp. 2681-2699, 2004.

[11] Fernández-Jimenez, A., Puertas, F., Effect of activator mix on the hydration and strength behavior of alkali-activated slag cements, Adv Cem Res 15, pp. 129-136, 2003.

[12] Aperador, W., Mejía De Gutiérrez R., Bastidas, D. M., Corrosion resistance of carbonated alkali-activated slag concrete, Corros Sci, 51, pp. 2027–2033, 2009.

[13] Torres, R., Aperador, W., Vera, E., Mejía De Gutiérrez, R., Ortiz, C. Estudio de la corrosión del acero embebido en concreto AAS sometido a cloruros, Dyna, Año 77, Nro. 164, pp. 5259, 2010.

[14] Rodríguez, E., Bernal, S., Mejia De Gutiérrez, R., Puertas, F., Alternative concrete based on alkali-activated slag, Mater Construcc 58, pp. 53-67, 2008.

[15] Puertas, F., Cementos de escorias activadas alcalinamente: Situación actual y perspectivas de futuro, Mater Construcc 45 pp. 53-64. (1995)

[16] Bastidas, D.M., González J.A., Feliu, S., Cobo, A., Miranda, J.M., A quantitative study of concrete-embedded steel corrosion using potentiostatic pulses, Corrosion 63, pp. 1094-1100, 2007.

[17] Bastidas, D.M., Cobo, A., Otero E., González, J.A. Electrochemical rehabilitation methods for reinforced concrete structures: advantages and pitfalls, Corros Eng Sci Techn 43, pp. 248-255, 2008.

[18] ASTM C 989-99 Standard, Standard specification for ground granulated blast-furnace slag for use in concrete and mortars, West Conshohocken, PA, American Society for Testing and Materials, 1999.

[19] ASTM C 150-02 Standard, Specification for Portland cement test, West Conshohocken, PA, American Society for Testing and Materials, 2002.

[20] ASTM A 706-08 Standard, Standard specification for low-alloy steel deformed and plain bars for concrete reinforcement, West Conshohocken, PA, American Society for Testing and Materials, 2008.

[21] ASTM C 876-99 Standard, Standard test for half-cell potentials of uncoated reinforcing steel in concrete, West Conshohocken, PA, American Society for Testing and Materials, 1999.

[22] Stern, M., Geary, A.L., Electrochemical polarization I. A theoretical analysis of the shape of polarization curves, J Electrochem Soc 104, pp. 56-63, 1957.

[23] Durar Network, Manual de Inspección, Evaluación y Diagnóstico de Corrosión en Estructuras de Hormigón Armado, CYTED Programe, Rio de Janeiro, 1997.

[24] Schiessl, P., (Editor), New Approach to Durability Design-An example for carbonation inducced corrosion, Comité Euro-International du Béton, CEB Bulletin, No. 238,

Lausanne, Switzerland, 1997.

[25] Yoon, I.S., Copuroglu, O., Park, K.B., Effect of global climate change on carbonation progress of concrete, Atmos Environ 41, pp. 7274-7285, 2007.

[26] Puertas, F., Palacios, M., Vázquez, T., Carbonation process of alkali-activated slag mortars, J Mater Sci 41, pp. 3071-3082, 2006.

[27] Wang, S.D., Scrivener, K., Hydration products of alkali activated slag cement, Cement Concrete Res 25, pp. 561-571, 1995.

[28] Palacios, M., Puertas, F., Effect of carbonation on alkali-activated slag paste, J Am Ceram Soc 89, pp. 3211-3221, 2006.

[29] Feliu, V., González, J.A., Andrade, C., Feliu, S. Equivalent circuit for modelling the steel-concrete interface. I. Experimental Evidence and theoretical predictions, Corros Sci 40, pp. 975-993, 1998.

[30] Bastidas, D.M., Interpretation of impedance for pores electrodes and diffusion processes, Corrosion 63, 515-521, 2007.